

Nanoscale Advances

Accepted Manuscript

This article can be cited before page numbers have been issued, to do this please use: A. Yadav, V. Agrahari, Y. Pihosh, M. Nakabayashi, W. Nogala, B. Giri, K. Domen, D. S. Pandey, B. Gupta and S. Sadhu, *Nanoscale Adv.*, 2024, DOI: 10.1039/D4NA00479E.



This is an Accepted Manuscript, which has been through the Royal Society of Chemistry peer review process and has been accepted for publication.

Accepted Manuscripts are published online shortly after acceptance, before technical editing, formatting and proof reading. Using this free service, authors can make their results available to the community, in citable form, before we publish the edited article. We will replace this Accepted Manuscript with the edited and formatted Advance Article as soon as it is available.

You can find more information about Accepted Manuscripts in the [Information for Authors](#).

Please note that technical editing may introduce minor changes to the text and/or graphics, which may alter content. The journal's standard [Terms & Conditions](#) and the [Ethical guidelines](#) still apply. In no event shall the Royal Society of Chemistry be held responsible for any errors or omissions in this Accepted Manuscript or any consequences arising from the use of any information it contains.

Impact of Polymorphism vs Shape of Titania Nanocrystals towards Hydrogen Evolution Reaction

Ankur Yadav^a, Vivek Kumar Agrahari^a, Yuriy Pihosh^b, Mamiko Nakabayashi^c, Wojciech Nogala^d
Balendu Sekhar Giri^e, Kazunari Domen^{b, g}, Daya Shankar Pandey^a□, Bhavana Gupta^{d, f}□, Subha
Sadhu^a□

^aDepartment of Chemistry, Institute of Science, Banaras Hindu University, Varanasi, India

^bOffice of University Professors, The University of Tokyo, 7-3-1 Hongo, Bunkyo-ku, Tokyo 113-8656, Japan

^cInstitute of Engineering Innovation, School of Engineering, The University of Tokyo, 7-3-1 Hongo, Tokyo, 113-8656, Japan

^dInstitute of Physical Chemistry, Polish Academy of Sciences, Kasprzaka 44/52, 01-224 Warsaw, Poland

^eSustainability Cluster, School of Advanced Engineering, UPES, Dehradun, India.

^fDepartment of Chemistry, Cluster of Applied Sciences, School of Advanced Engineering, UPES, Dehradun, India

^gResearch Initiative for Supra-Materials (RISM), Shinshu University, 4-17-1 Wakasato, Nagano 380-8533, Japan

□ Email: subha@bhu.ac.in; bhavana.gupta@ddn.upes.ac.in; dspbhu@bhu.ac.in

Abstract

In this report, we investigated the impact of polymorphism vs dimension control of titania nanocrystals towards hydrogen generation. Two different forms of titania nanoparticles have been synthesized following solvothermal method leading to the formation of two distinct physicochemical features. Detail structural, morphological, and optical studies revealed the formation of titania nanorods correspond to rutile while granular particles correspond to anatase phase. Among various titania polymorphs anatase is well known for superior photocatalytic activity but to our surprise, the as-synthesized rutile nanorods exhibited higher catalytic activity in comparison to anatase spheres and hydrogen evolution was significantly enhanced after addition of diminutive amount of Pt as co-catalyst. Thus, despite of higher catalytic activity of anatase, the enhanced hydrogen evolution of rutile nanorods may be related to the creation of a 1D structure.



Our study highlights the importance of considering not only TiO₂ polymorphism, but also shape and dimension, in optimizing photocatalytic H₂ production.

Keyword: Photocatalysis; TiO₂, Nanoparticle; water splitting, Polymorphism

Introduction:

Hydrogen fuel is one of the promising and reliable sources of green energy and can photocatalytically be produced from water utilizing solar light [1, 2]. For the first time, Fujishima and Honda reported the formation of gaseous hydrogen (H₂) through photoelectrochemical (PEC) water splitting, using titania (TiO₂) as photoelectrode [3]. After this report, different research groups have extensively explored water splitting in the presence of diverse photoelectrodes [4-6]. Over the last ten years, TiO₂ has been widely studied for PEC due to its stability, unique optoelectronic properties, and nontoxicity [7-9]. Owing to the difference in electronic structure, the physiochemical properties of titania largely depend on crystallinity, shape, and size [10]. Amongst the polymorphs of titania *i.e.* anatase, rutile, and brookite, the first two are most often used for water splitting reactions as catalysts. Extensive studies on different polymorphs of titania have revealed that anatase shows superior photocatalytic activity related to rutile [11]. Various factors, such as the stability of the compound in aqueous solution under UV irradiation, superior oxidizing and reducing properties, and the band gap of the material, significantly influence photocatalytic performance [12]. The band gap of anatase (3.2 eV) exceeds that of rutile (3.0 eV), resulting in reduced photon absorption for water splitting. Even though the enhanced photocatalytic activity and water splitting efficiency of the anatase phase occur due to the presence of valence band maximum at higher energy level with respect to the redox potential of the adsorbed molecules [13-14]. In addition, along with the direct band gap, anatase also exhibits a lower indirect band gap, thus facilitating exciton generation. Semiconductors with indirect band gap often have higher charge carrier lifetime, accelerating efficient water splitting [15-17]. Besides, charge transport properties vary in individual polymorphs as a consequence of different crystal structures.

Along with polymorphism, photocatalytic activity also depends on the shape and size of the semiconductor material. One-dimensional (1D) structures with varying dimensionalities, such as nanorods, nanotubes, nanowires, etc., appeal to photocatalysts owing to their anisotropy and the presence of less grain boundary, assisting efficient charge transport. It is well established that



photogenerated electron transport and collection are more effectively achieved with nanorod and nanowire arrays [18-23]. The photocatalytic performance of mixed-phase titania, including rutile and anatase nanotubes, nanorods, and nanosquares, was investigated for solar hydrogen production. It was observed that titania nanotubes exhibited a two-fold enhancement in hydrogen production compared to nanosquares [24]. In a separate study, Murakami et al. synthesized decahedral anatase titania with particle sizes ranging from 25 to 60 nm, finding that 40 nm particles demonstrated superior photocatalytic activity due to optimally enhanced surface area and efficient separation of redox sites [25]. The thermodynamic stability of the anatase phase is higher when the particle size is less than 11 nm, while for the rutile phase, the stability of the compound increases when the particle size is more than 35 nm. Particles with smaller sizes are known to absorb more visible light and have lower electron-hole recombination [26].

The impact of size on photocatalytic hydrogen generation has been previously studied independently [27-28]. However, to the best of our knowledge, the combined influence of the polymorph of TiO₂ and shape has not been thoroughly investigated. Though extensive studies revealed that anatase exhibits superior photocatalytic activity compared to other phases, it is important to know the impact of shape over polymorphism. What will be the effect on catalytic activity if 1D rutile nanocrystals are used instead of anatase? Does rutile have higher photocatalytic activity? To find the answer, in this present report, we synthesize various shapes of titania polymorphs and investigate their photocatalytic activity towards hydrogen production. Anatase nanosphere and rutile nanorod were synthesized by solvothermal method, and the resulting systems were thoroughly characterized for their effectiveness in the hydrogen evolution reaction (HER). Our findings revealed that rutile nanorods exhibited three times higher catalytic activity compared to anatase nanospheres, leading to greater hydrogen generation through photocatalyst. It is well established that pure titania struggles to generate hydrogen in aqueous systems; consequently, researchers often utilize sacrificial reagents or noble metals, such as gold, palladium, or platinum, as co-catalysts to facilitate hydrogen evolution [12,29]. In our study, we employed 0.1 wt.% platinum as a co-catalyst and observed a significant enhancement in the photocatalytic hydrogen evolution rate in rutile titania, with a boost in production rate of 30 times compared to the absence of a co-catalyst. Our study highlights the importance of comparative study of titania polymorphs and dimension to optimize photocatalytic H₂ production.



Experiment:**Synthesis:**

Titanium tetra chloride (TiCl_4) was procured from Merck India Ltd while potassium tetra chloroplatinate ($\text{K}_2[\text{PtCl}_6]$) and titanium butoxide ($\text{Ti}(\text{O-Bu})_4$ (Purity 97%,) were obtained from Aldrich. On the other hand, common solvents like ethanol, methanol, toluene and hydrochloric acid (HCl) were procured from Aldrich.

The synthesis procedure of two different shape TiO_2 nanoparticles is illustrated in **Figure 1**. To synthesize TiO_2 nanorod 5 mL toluene was taken in a clean Teflon cup, followed by the addition of 0.3 M titanium butoxide ($\text{Ti}(\text{O-Bu})_4$) and 1M titanium tetrachloride (TiCl_4). After 30 minutes of stirring at room temperature, 0.5 mL of concentrated HCl was added to the solution. Again, the mixture was stirred for 30 min and the Teflon cup containing the mixture was kept in steel autoclave and put inside a muffle furnace at 180°C for 9 hr. After the completion of the reaction, the product in the form of a precipitate was collected, washed in ethanol, and centrifuged. After centrifugation, the precipitate was dried in an oven at 60°C and the dried powder was used for further characterization. Similarly, TiO_2 granular particle was synthesized using ethanol as a solvent instead of toluene, $\text{Ti}(\text{O-Bu})_4$ as the precursor and oleic acid and oleyl amine as the capping agent. 6 ml ethanol, 0.8 M $\text{Ti}(\text{O-Bu})_4$, 4.2 M oleic acid, and 4.2 M oleyl amine was added in a Teflon cup to prepare the solution and the solution was stirred for 30 min. Subsequently, the solution was kept in an autoclave at 180°C for 18hr. After completion of the reaction, the product in form of a precipitate was washed, centrifuged, and dried.



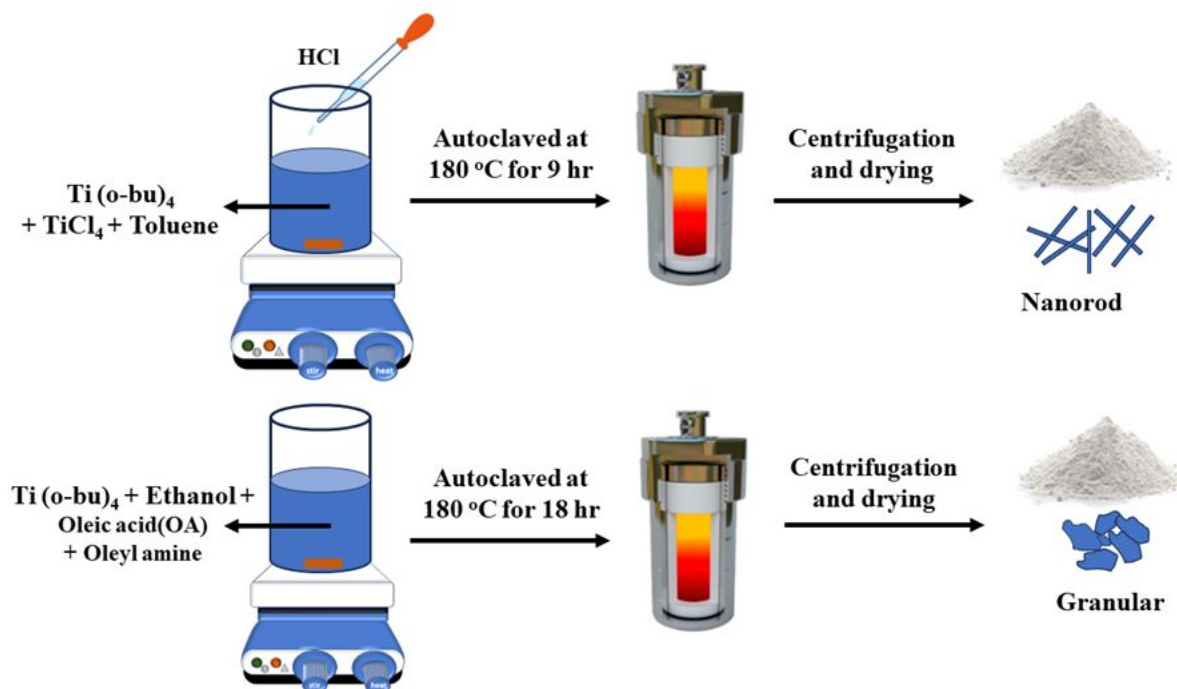


Figure 1: Schematic of synthesis of TiO₂ nanoparticle in two different morphologies.

Characterization:

The crystal structure of the as-synthesized TiO₂ was determined by X-ray diffraction (XRD) (Smart Lab., Rigaku, Japan), equipped with CuK α ($\lambda = 1.5406 \text{ \AA}$) irradiation source and operated at 45kV and 200mA. The step size was 0.02°. The Raman spectra were acquired using a LabRam HR evolution spectrometer (manufacturer: Horiba). The samples were excited by a 532nm laser line (He-Ne laser) operating at a power of 30 mW, utilizing a grating with 600 grooves/mm.

To study the morphology of the TiO₂ nanoparticles, scanning electron microscopy (SEM) (SU8020, Hitachi, Japan) and transmission electron microscopy ((S)TEM, JEM-2800, JEOL, Japan) characterization was performed using X-MAX 100 TLE SDD detector operating at 200 kV. High resolution TEM (HR-TEM) images were analyzed in Gatan Digital Micrograph 2.3 software. Elemental composition maps were acquired within 10 keV channel with a resolution of 0.64 nm/px and a dwell time of 8192 μ s using the Bruker Xflash detector with 129 eV energy resolution. The optical properties of TiO₂ nanoparticles were studied by FTIR and UV-visible diffuse reflectance spectroscopy (UV-vis-DRS) using (FIR, Perkin Elmer) and (V-670, Jasco, Japan) instruments respectively.



The PEC properties of the TiO₂ thin films photoelectrodes were investigated using a three-electrode system with the specimen, Ag/AgCl in a saturated aqueous KCl solution, and a Pt wire connected to a potentiostat (Autolab model) as working, reference, and counter electrodes. TiO₂ thin films photoelectrodes were fabricated using TiO₂ dispersion in isopropanol (20 mg in 50 μ l). This dispersion was cast on an exposed area of ITO control by scotch tape boundary. 0.5 M Na₂SO₄ (pH 7) was used as an electrolyte. A Xenon lamp (lumen 200) of 25 percent intensity shining 60 Lumen (40 mW/cm²) of light on the electrode was used as light source. Each PEC measurement was performed under Ar ambient in a gas-tight cell with an optical window.

Photocatalytic H₂ generation:

For the photocatalytic generation of hydrogen, 20 mg of TiO₂ powder was dispersed in a 40 ml mixture of methanol and water (with a ratio of 80:20), with and without the addition of 0.1 % Pt. The addition of platinum was achieved via photodeposition. Specifically, 5 μ L of a 20 mM K₂PtCl₆ solution was added to the TiO₂ dispersion in a methanol-water mixture, with a total volume of 40 mL, and a composition identical to that previously mentioned. The hydrogen gas generation was monitored until the deposition process was completed. The dispersion was achieved through sonication to ensure homogeneity. Subsequently, the prepared substances were placed in a Pyrex reactor, which was top-illuminated and connected to a closed gas circulation system. All photocatalytic reactions were conducted at 288K under a background pressure of 5 kPa. To eliminate any air present in the reaction mixture, evacuation was carried out before introducing Ar gas to establish a background pressure of approximately 5 kPa. The reactant solution was then exposed to irradiation from a 300 W Xe-lamp. The distance from lamp to the sample is 10 cm. The gaseous products generated during these reactions were analyzed using an integrated online gas chromatography system. The system consisted of a chromatograph (GC-8A Shimadzu, Japan) equipped with molecular sieve 5 Angstrom columns and a thermal detector, with Ar serving as the carrier gas.

Results and discussion:

The as-synthesized nanoparticles by a solvothermal method employing diverse solvents, precursors and capping agents are expected to have distinct phases and shapes. The difference in shape and structure characteristics of the nanoparticles can significantly impact their optical and



other physicochemical properties. XRD and Raman studies have been performed to verify the crystal structure and phase of the nanoparticles (**Figure 2 a and b**). Diffraction at an angle of 25.3° and 27.5° , are indexed for the anatase (101) and rutile (110) phase of TiO_2 , respectively [30, 31]. Also, (101) and (211) diffraction plane of the rutile phase at 36.2° and 54.6° was observed, whereas the diffraction pattern at 48.1° and 54.9° correspond to (200) and (105) plane of anatase is detected. It was observed that the XRD peak for anatase is broader than that for the rutile, which can be attributed to the smaller crystallite size of anatase. As crystallite size decreases, the peaks in the XRD pattern tend to broaden. Figure S1 presents the TEM images of the as-synthesized nanoparticles, revealing crystallite sizes of ~ 10 for anatase granular particles and 40nm for rutile nanorods, thereby supporting the findings from XRD analysis. Due to its smaller crystallite size, anatase exhibits a higher surface area compared to rutile nanorods. The Brunauer–Emmett–Teller (BET) analysis indicates observed surface area of $36.02 \text{ m}^2/\text{g}$ for anatase and $14.76 \text{ m}^2/\text{g}$ for rutile, as shown in **Figure S2**. Therefore, the as-synthesized anatase granular particles possess a greater surface area than the rutile nanorods. Rutile nanorods are synthesized in the presence of hydrochloric acid (HCl) and titanium precursors ($\text{TiO}(\text{Bu})_4$ and TiCl_4), which exhibit differing rates of hydrolysis, with toluene serving as the solvent. A combination of various titanium precursors and HCl is introduced into the reaction vessel containing toluene to modulate the hydrolysis rate and facilitate the rapid precipitation of titanium hydroxides. The primary role of HCl is to regulate the hydrolysis rate, thus preventing the rapid precipitation of titanium hydroxide. The hydrolyzed precursors significantly influence the growth and morphology of the resulting nanocrystals [28, 29].

As the temperature increases, H^+ ions are released from the hydrolyzed precursor, leading to the formation of hydrated titanyl ions through intramolecular oxolation. Subsequently, with further elevation of temperature and pressure within the hydrothermal reactor, condensation of the hydrated titanyl ions occurs, resulting in the formation of TiO_6 octahedra through the edge-sharing of hydrated titanyl ions in the equatorial position. Thereafter, rutile nanorods are formed through the polymerization of octahedra, crystallizing into a one-dimensional structure along the c-axis. Previous studies have shown that when only TiCl_4 is utilized as a precursor, faceted truncated bipyramidal nanocrystals are obtained. Conversely, the exclusive use of $\text{Ti}(\text{OBu})_4$ leads to the formation of an agglomerated film [33]. Therefore, both TiCl_4 and $\text{Ti}(\text{OBu})_4$ precursors are essential for the successful formation of rutile nanorods.



The formation and purity of the anatase and rutile phase nanocrystals were confirmed through X-ray diffraction (XRD) analysis, which indicated the absence of additional peaks corresponding to impurities. Granular anatase nanocrystals are generated in the presence of capping agents, specifically oleic acid and oleylamine, which bind to high-energy facets during nucleation and facilitate the formation of granular nanoparticles [34, 35]. Previous reports indicated that oleic acid and oleylamine exhibit differing binding strengths: oleic acid binds more strongly to the {001} facets of anatase, while oleylamine preferentially attaches to the {101} facets. This selective binding suppresses growth in the corresponding directions, thereby promoting the formation of nanospheres [36]. The formation and purity of the anatase and rutile phase nanocrystals were affirmed by XRD analysis, which clearly showed the absence of additional peaks due to impurity. Granular anatase nanocrystals are formed in the presence of capping agents (oleic acid and oleylamine), which are used to attach to the high energy facets during nucleation and promote the formation of granular nanoparticles [34, 35]. It was reported earlier that oleic acid and oleylamine have different binding strengths where oleic acid binds strongly to {001} facets of anatase whereas oleylamine attaches to {101} facets. Hence, the selective binding hinders the growth in corresponding direction and aid the formation of nanosphere [36].

The formation of pure phase anatase and rutile nanoparticles has also been confirmed by Raman analyses (**Figure 2b**). The granular anatase nanoparticles displayed characteristic peaks at 144, 396, 515 and 637 cm^{-1} corresponding to E_g , B_{1g} , A_{1g} and E_g vibration modes, respectively. Conversely rutile nanorods exhibited characteristic Raman active fundamental vibration at 439 and 606 cm^{-1} correspond to E_g and A_{1g} mode, along with second order vibration at 146 cm^{-1} . The E_g and A_{1g} vibration modes are caused by the asymmetric bending and symmetric stretching of the O-Ti-O bond along {001} and {110} planes, respectively [37].

FTIR spectra provided additional structural information of the nanoparticles (**Figure S3**). The crystallinity of the material can be correlated with the peak intensity between 750 and 1000 cm^{-1} , with anatase exhibiting greater intensity related to the rutile phase, probably due to nanocrystallization/defect centre during hydrothermal synthesis. [38]

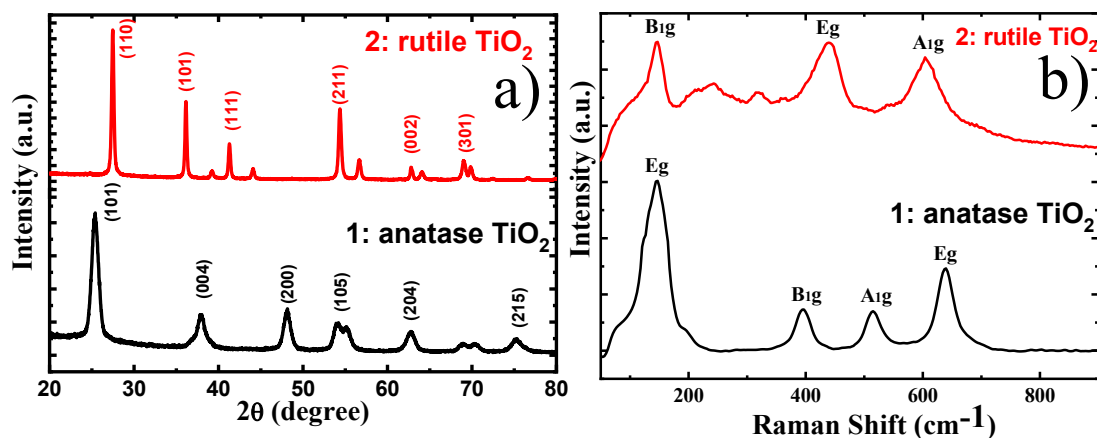


Figure 2: a) XRD pattern and b) Raman spectra of anatase granular (1) and rutile TiO₂ nanorod (2).

Following the confirmation of the formation of pure anatase and rutile nanoparticles, our research aimed to investigate the optical properties and band structure of the as-synthesized compounds, as the band gap of these materials plays a crucial role in H₂ generation [29, 39-40]. The band gap was determined from UV-vis-DRS spectra using Kubelka-Munk's function (**Figure 3**), revealing values of 3.2 eV for anatase and 3 eV for rutile. The sharp transition observed near the band edge is attributed to the electronic transition from the valence band of O_{2p} to the conduction band of Ti_{3d}. Interestingly, the rutile phase exhibited a 0.2 eV lower band gap compared to the anatase phase, in line with earlier report [41].



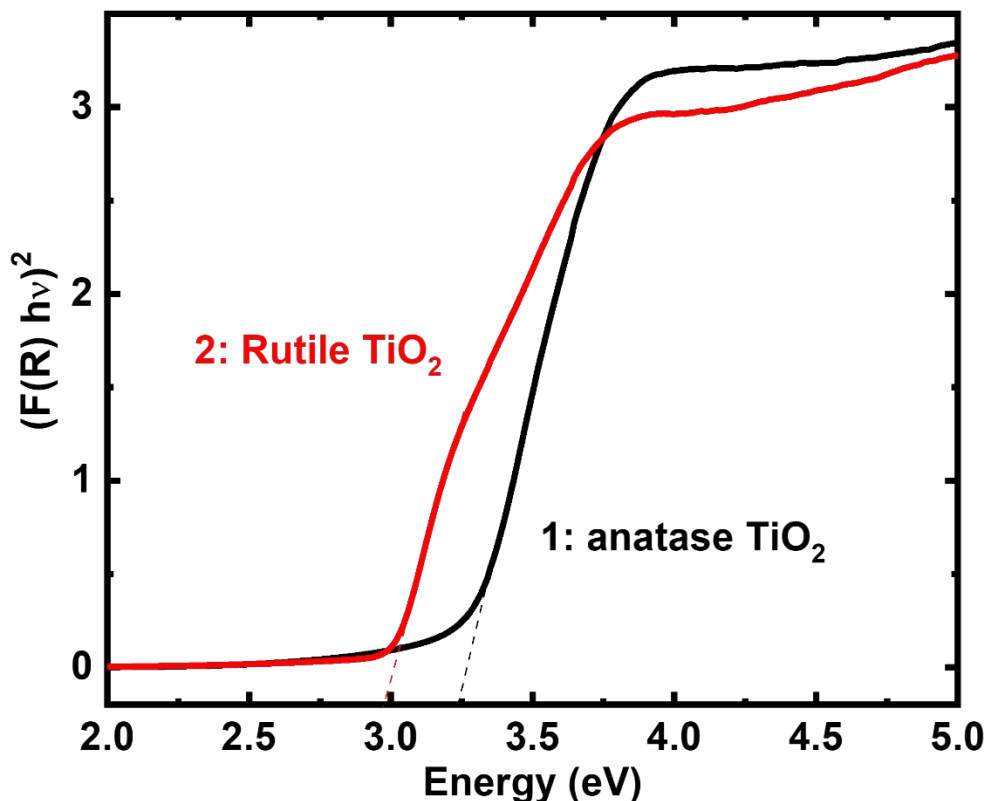


Figure 3: Band gap determination of as-synthesized anatase granular (1) and rutile TiO₂ nanorod (2) from UV-vis-DRS spectra using Kubelka Munk function.

It is hypothesized that the low band gap observed in the rutile phase TiO₂ is due to a downward shift in the conduction band energy. Enhanced H₂ generation is most effectively achieved with a low band gap; however, the catalytic performance is also influenced by other physicochemical characteristics. Therefore, a comprehensive study of the surface properties, morphology, and photoelectrochemical characteristics is essential before investigating the photocatalytic H₂ evolution feature.

The crystalline phase and shape of TiO₂ can be controlled by the choice of solvent, precursor, and capping agent. **Figures 4 a** and **b** illustrate that the use of a capping agent in ethanol yields granular anatase TiO₂ nanoparticles, while TiO₂ nanorods are obtained without a capping agent in toluene. Energy-dispersive X-ray spectroscopy (EDAX) mapping reveals a uniform distribution of titanium (Ti) and oxygen (O) across the surface, along with the calculation of the atomic weight percentages of these elements (see **Figures 4c, 4d**, and supporting information **Figure S4**) Notably, the solvent used in the synthesis influences nanoparticles morphology and surface properties and impacts the O/Ti ratio, as shown in **Figure. 4a** and **b-Inset**. Rutile phase TiO₂ nanorods exhibit a higher O/Ti



ratio compared to anatase phase TiO_2 spheres. The oxygen-to-titanium (O/Ti) ratios were also determined using X-ray photoelectron spectroscopy (XPS), yielding values 1:2.04 for anatase granular and 1: 2.40 for rutile nanorods. These results are consistent with the trends observed in the EDAX analysis. The XPS spectra and the calculations of the O/Ti ratios are provided in the supporting information (**Figure S5, S6 and Table S1**).

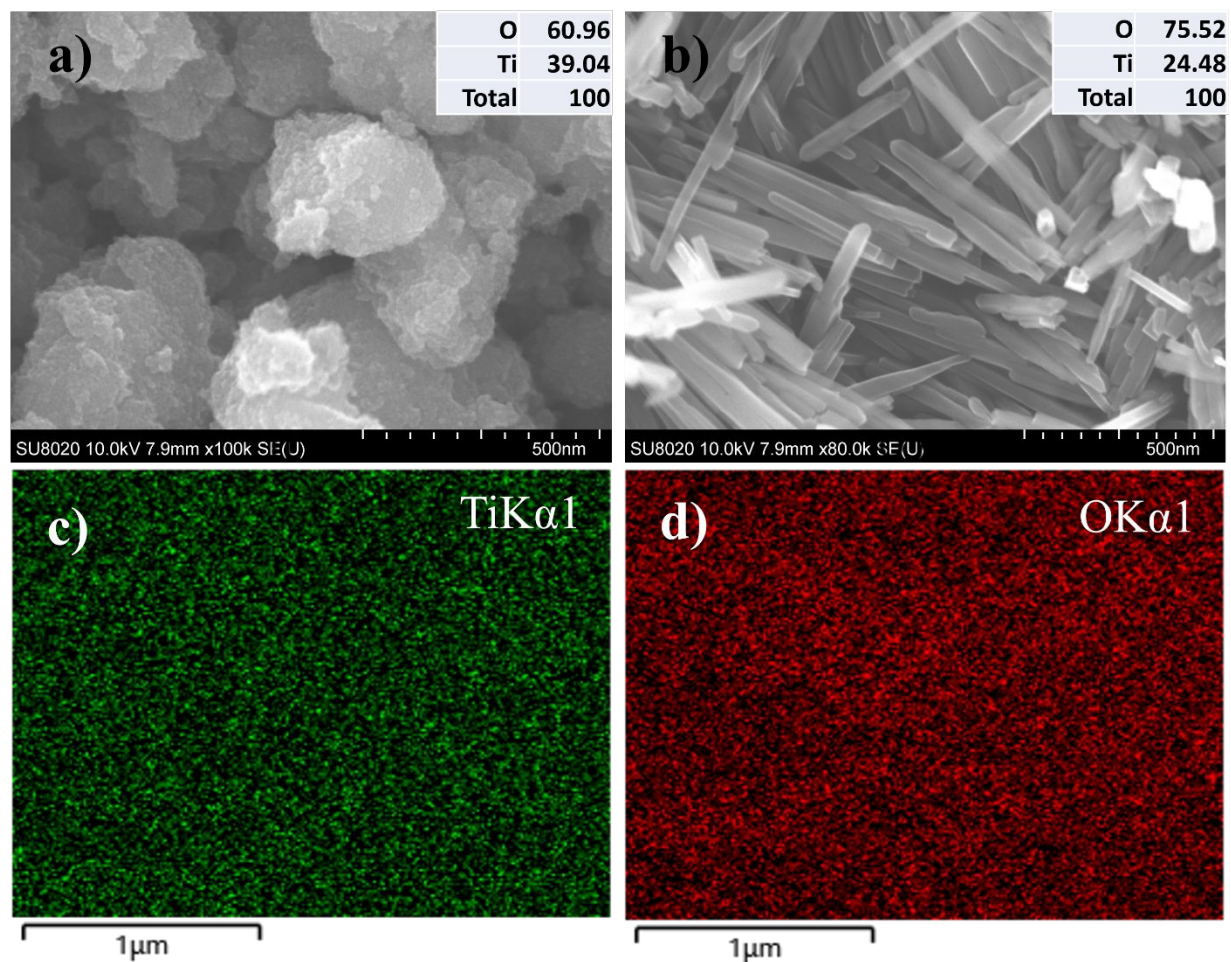


Figure 4: SEM images of a) anatase granular and b) rutile TiO_2 nanorod (Inset-atomic percentage of Ti and O). c) Ti and d) O mapping of TiO_2 nanorod surface.

The resistivity of TiO_2 is strongly correlated with the ratio of O/Ti. The material's resistivity increases with a larger ratio and vice versa. Increased resistivity has an adverse effect on the electron transfer, or charge transfer, that occurs during photocatalysis. [42] However, because the path for charge transport is shorter in nanostructure shape, photocatalysis benefits from shorter path length during photocatalysis [43]. The Ti and O ratios for TiO_2 rutile (nanorod) and TiO_2



anatase (granular) were found to differ based on the EDAX mapping. This difference in ratio ultimately affects the overall electron transfer to the adjacent moiety in water (photocatalysis) or electrode (photo-electrocatalysis) and competes with the effect of path length.

Following particle transfer on an ITO surface at equal amounts and surface area, photoelectrochemical studies were conducted utilizing voltametric and impedance techniques (as depicted in **Figure 5 a** and **b**) to assess charge transfer resistance. [44] Rutile TiO₂ exhibited approximately three times higher catalytic current under light irradiation compared to anatase TiO₂ using linear sweep voltammetry (LSV). Consistent results were observed in impedance measurements via Nyquist plot, demonstrating a charge transfer resistance in TiO₂ rutile three orders of magnitude lower than in TiO₂ anatase. A significant current was observed in case of TiO₂ nanorods, likely due to efficient charge transfer from the materials to the electrode surface, facilitated by charge generation in the presence of light. The increased charge production can be attributed to the enhancement of diffusion length in the nanorods, which effectively compensates for the effects of charge recombination.

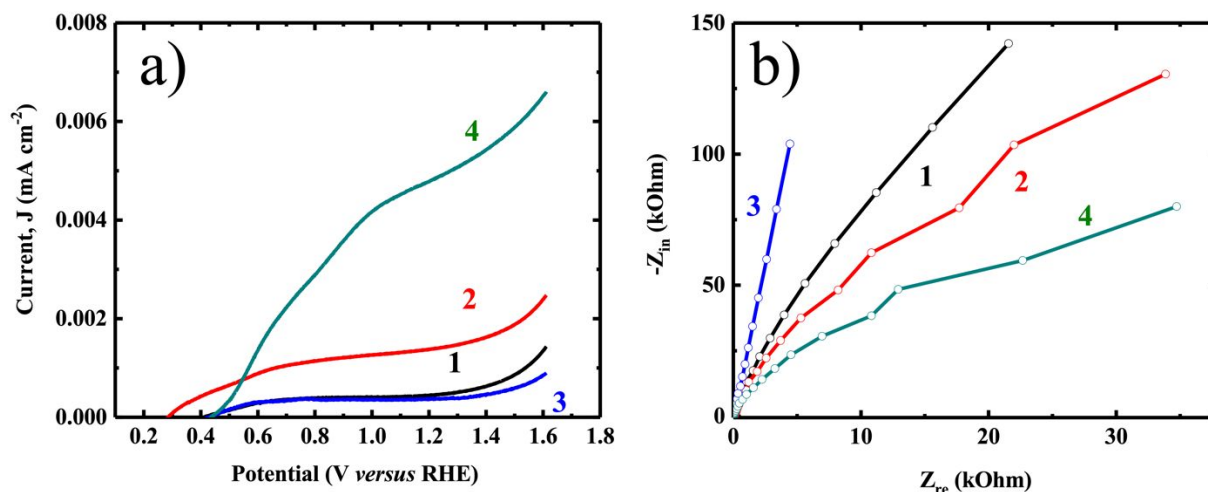


Figure 5: a) LSV and b) Nyquist plot of anatase granular (1-dark 2-light) and rutile TiO₂ nanorod (3-dark 4-light)

It can be inferred that the ratio of O/Ti plays a significant role in determining the resistivity of materials. Additionally, the morphology and band gap are important in influencing charge mobility and separation within the matrix. The results suggest that photocatalytic H₂ evolution will be much higher in the case of rutile TiO₂ compared to anatase TiO₂.



In order to evaluate the efficiency of photocatalytic H₂ generation and understand the influence of various physicochemical parameters, the as-synthesized TiO₂ nanoparticles with different morphology were further examined. The results depicted in **Figure 6a** reveal that the TiO₂ nanorod morphology exhibited a higher rate of H₂ generation (average 1.2 μmol/h and highest 3 μmol/h) compared to the TiO₂ granular morphology (average 0.8 μmol/h and highest 1 μmol/h). The sustained stability of the nanorod during four hours of hydrogen production is evidence of the consistent rate of hydrogen evolution observed over three consecutive cycles (**Figure. 6b** supporting information **Figure S7**). This enhanced performance can be attributed to the superior dispersion of the nanorods due to their smaller size, which facilitates efficient light absorption and charge separation (**Figure S8 a-c**). Thus, the size and dimensions of TiO₂ play a significant role in enhancing H₂ production. The morphology of TiO₂ nanorods aids in the efficient separation of light-generated charges due to their shorter surface diffusion length. Previous studies have indicated that various physicochemical properties affect the generation of H₂ on TiO₂ surfaces, with shape and size emerging as key factors in this process [29,39]

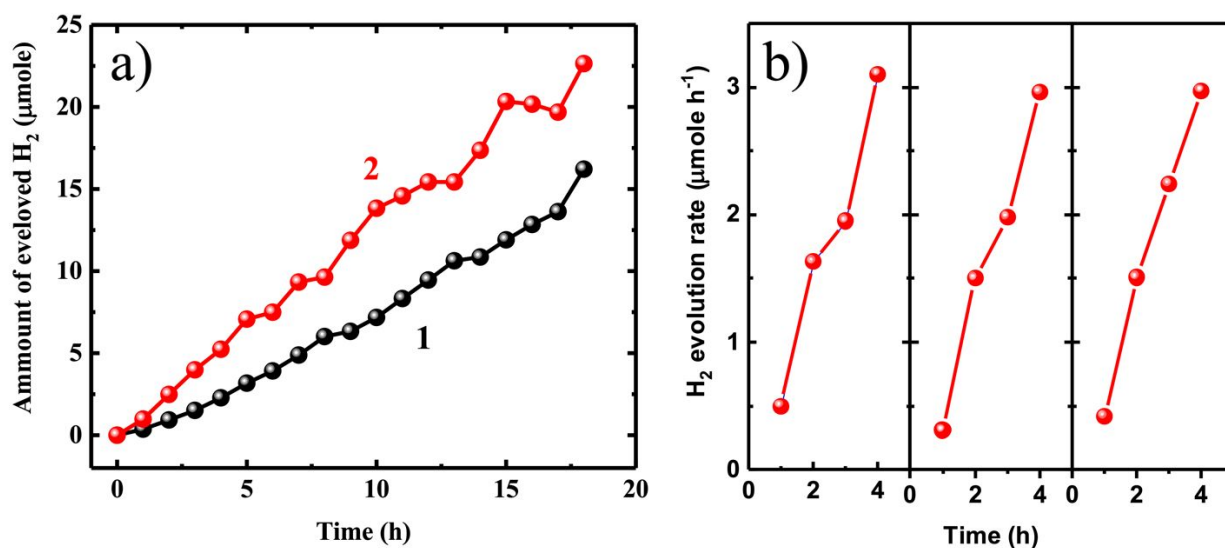


Figure 6: a) Photocatalytic H₂ generation under 300 W Xe-lamp for 1) anatase granular and 2) rutile TiO₂ nanorod b) three consecutive runs until maximum rate of H₂ generation.

As evidenced from the results above, the nanorod morphology of TiO₂ is beneficial for improving charge separation, a process which can be further optimized through the inclusion of a surface co-catalyst layer. TiO₂ nanorods were modified with 0.1 wt. % of Pt to enhance charge separation during hydrogen production. The simultaneous deposition of Pt (in form of nanoparticles) during hydrogen production, which eventually reached a plateau at 90 μmol/h highest rate of H₂



generation while average rate is 50 $\mu\text{mol/h}$ once Pt deposition was complete. This suggests that the co-catalytic effect of the charge transfer from the TiO_2 surface is enhanced in the presence of Pt nanoparticles, as illustrated in (**Figure S8 d**).

Figure 7a displays the low-resolution TEM image of the TiO_2 rutile sample with Pt deposited on TiO_2 nanorod. Distribution of Pt is partly (less than 10 percent) covering the surface of TiO_2 nanorod surface (Supporting information S9). This clearly supports the increase in the H_2 evolution with increasing the amount of Pt from 0.1 wt. % to 1 wt. %. Lattice fringes with interplanar distances of ~ 0.32 nm corresponding (110) plane are observed in **Figure 7 b**, consistent with literature values [45]. The sharp and ordered selected area electron diffraction (SAED) pattern in **Figure 7 c** along [001] zone axis confirms the single crystalline nature of the rutile nanorods. High-resolution TEM reveals uniform deposition of 2-4 nm Pt nanoparticles in small patches on the surface of TiO_2 nanorod, as depicted in **Figure 7a**. Elemental mapping in **Figure 7d-f** further verifies the distribution of Pt on the nanorod surface. The nanorod structure provides a larger surface area for a precise and thin layer of Pt deposition, preventing agglomeration and significantly enhancing H_2 generation. The morphological characterization of the nanorods was performed after hydrogen evolution experiment (**Figure S9 and Figure S10**), and no observable changes in shape were detected. This indicates that the nanorods exhibit high photocatalytic



stability.

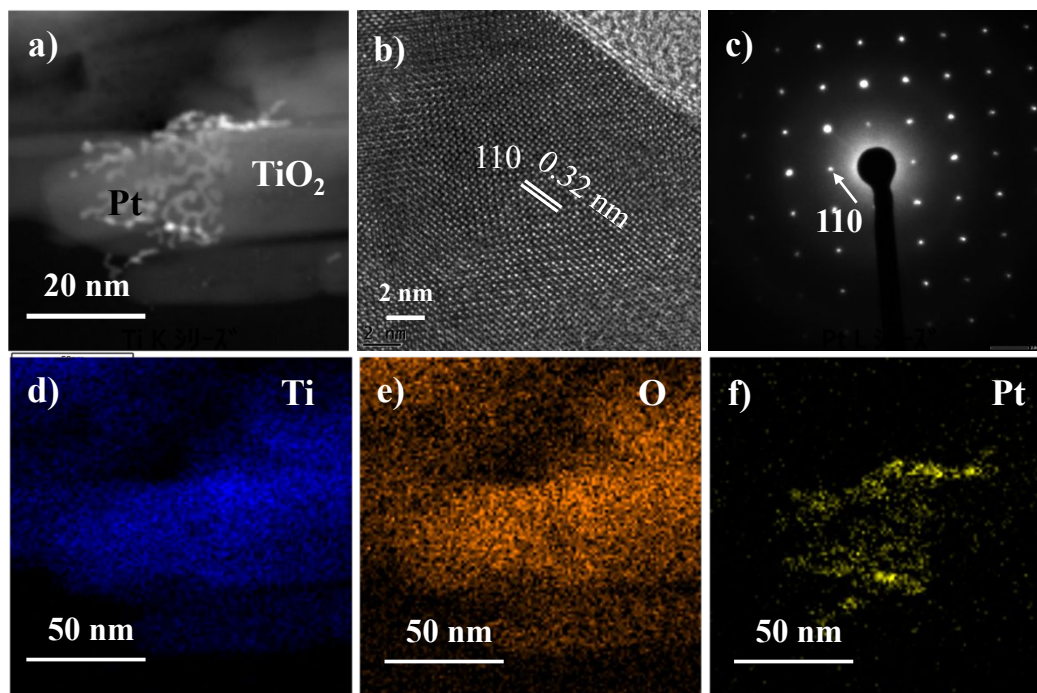


Figure 7: (a) ADF STEM image of rutile TiO₂ nanorod after Pt deposition. (b) HRTEM image taken on the surface of rutile TiO₂ particle (c) SAED pattern from the rutile TiO₂ particle confirming the formation of single crystal and d)-f) elemental mapping for Ti, O, and Pt, respectively.

Since the influence of Pt on H₂ generation is already well established in the literature, our result is compared with previous studies and illustrated in **Table 1**. The table demonstrates that the unique nanorod morphology facilitates cocatalyst deposition for enhanced H₂ production using minimal Pt, in contrast to prior studies requiring larger amounts of Pt. This effect is observed even in the less favorable rutile phase of TiO₂.



Table 1 A summary of the key findings of Pt-doped TiO₂ photocatalysts reported in recent years for H₂ production.

Pt loading on TiO ₂	Light Source	Crystalline phase of TiO ₂	Photocatalyst loading (mg)	H ₂ production efficiency	Quantum efficiency	Reference
Pt-5 wt %	500 W Hg-Xe lamp with dichroic filter (280–400 nm)	Anatase-Rutile bulk	500 mg in 1 L in 1:9 MeOH/H ₂ O medium	27.6 mmol g ⁻¹ h ⁻¹	5.6 %	[46]
Pt- 2.5 wt %	Black Light Blue Lamp of 15W	Anatase-Rutile bulk	150 mg in 1 L containing 2 vol.% ethanol	383 mmol h ⁻¹ g ⁻¹	7.8 %	[47]
Pt- 1.0 wt %	300 W Xe lamp	Anatase nanosheet	5 mg in 100 ml water containing 10 % methanol	5086 μmol h ⁻¹ g ⁻¹	-	[48]
Pt- 1.0 wt %	8 Philips CLEO 15 W	Anatase-Rutile bulk	200 mg in 200 ml water containing 25 vol.% methanol	1846 μmol h ⁻¹	-	[49]
Pt- 0.1 wt %	300 W Xenon lamp	Rutile nanorod	20 mg in 40 ml water containing 10 vol % methanol	Average 50 μmol h ⁻¹ highest 90 μmol h ⁻¹	Average 7.41 % Highest 10.11 %	Current work
Pt-1 wt %	300 W Xenon lamp	Rutile nanorod	20 mg in 40 ml water containing 10 vol % methanol	Average 150 μmol h ⁻¹ highest 250 μmol h ⁻¹	Average 22.23 % Highest 30.33 %	Current work

Conclusion:

In summary, this study underscores the significance of TiO₂ morphology and crystalline phase in photocatalytic water reduction. Notably, the results suggest that the charge carrier diffusion path plays a crucial role, and nanorods exhibit a distinct advantage due to their one-dimensional shape. Specifically, the experiments show a threefold increase in H₂ generation (3 μmol/h) in rutile nanorods compared to anatase nanosphere (1 μmol/h), suggesting that the 1D structure is more effective for hydrogen production. The enhanced photocatalytic activity in TiO₂ nanorods is attributed to improved charge mobility. Therefore, the charge mobilities and exciton lifetime of the photocatalyst should be taken into consideration when optimizing photocatalytic properties. Additionally, the uniform deposition of Pt cocatalyst on the nanorod surface further enhances



charge carrier mobility, resulting in a 30-40-fold increase in H₂ gas evolution (average 50 μmol/h and highest 90 μmol/h). This study paves the way for future research to explore the impact of nano dimensions on the photocatalytic performance of the most effective photocatalyst.

Acknowledgements:

B.G. acknowledges funding from the European Union's Horizon 2020 research and innovation programme under the Marie Skłodowska-Curie Grant Agreement No. 847413. Scientific work published as part of an international cofinanced project funded from the programme of the Minister of Science and Higher Education entitled "PMW" in the years 2020–2024; Agreement No. 5005/H2020-MSCA-COFUND/2019/2. This work was partially supported by "Advanced Research Infrastructure for Materials and Nano- technology in Japan (ARIM)" of the Ministry of Education, Culture, Sports, Science and Technology (MEXT), Grant Number JPMXP1223UT0004. S.S. acknowledges the financial support by the Department of Science and Technology, Government of India, under the DST Inspire Faculty Award (DST/INSPIRE/04/2021/000742). A.Y and V.K.A acknowledge the support from UGC for junior research fellowship.

Reference:

- [1] Q. Hassan, S. Algburi, A.Z.Sameen, H.M. Salman, M. Jaszczur. Green hydrogen: A pathway to a sustainable energy future. *Int. J. Hydrogen Energy*, 2024, **50**, 310-33.
- [2] K.K. Jaiswal, C.R. Chowdhury, D. Yadav, R. Verma, S. Dutta, K.S. Jaiswal, B. Sangme, K.S.K. Karuppasamy. Renewable and sustainable clean energy development and impact on social, economic, and environmental health. *Energy Nexus*, 2022, **7**, 100118.
- [3] K. Maeda. Photocatalytic water splitting using semiconductor particles: History and recent developments. *J. Photochem. Photobiol. C: Photochem. Rev.*, 2011, **12**, 237-68.
- [4] B. Gupta, A.A.Melvin, T. Matthews, S. Dash, A.K. Tyagi. TiO₂ modification by gold (Au) for photocatalytic hydrogen (H₂) production. *Renew. Sustain. Energy Rev.*, 2016, **58**,1366-75.
- [5] B. Gupta, A.A. Melvin, T. Matthews, S. Dhara, S. Dash, A.K. Tyagi. Facile gamma radiolytic methodology for TiO₂-rGO synthesis: Effect on photo-catalytic H₂ evolution, *Int. J. Hydrog. Energy*, 2015, **40**, 5815-23
- [6] G. Liao, C. Li, , S-Y Liu, B. Fang, H. Yang. Z-scheme systems: From fundamental principles to characterization, synthesis, and photocatalytic fuel-conversion applications. *Phys. Rep.*, 2022, **983**, 1–41.



- [7] S. Feizpoor, S.R. Pouran, A.H. Yangjeh. Recent progress on photocatalytic evolution of hydrogen gas over TiO₂-x-based emerging nanostructures, *Mater. Sci. Semicond. Process.*, 2023,**162**, 107444.
- [8] N.M. Gupta. Factors affecting the efficiency of a water splitting photocatalyst: A perspective, *Renew. Sustain. Energy Rev.*, 2017,**71**, 585-601.
- [9] D.R. Eddy, M.D. Permana, L.K. Sakti, G.A.N. Sheha, Solihudin, S. Hidayat, T. Takei, N. Kumada, I. Rahayu. Heterophase Polymorph of TiO₂ (Anatase, Rutile, Brookite, TiO₂ (B)) for Efficient Photocatalyst: Fabrication and Activity. *Nanomaterials*, 2023,**13**, 704.
- [10] J. Joo, S.G.Kwon, T. Yu, M. Cho, J. Lee, J. Yoon, T. Hyeon. Large-Scale Synthesis of TiO₂ Nanorods via Nonhydrolytic Sol–Gel Ester Elimination Reaction and Their Application to Photocatalytic Inactivation of *E. coli*. *J. Phys. Chem. B*, 2005,**109**, 15297-302.
- [11] T. Luttrell, T. S. Halpegamage, S. J.Tao, J.A.Kramer, A.E.Sutter, M.Batzill. Why is anatase a better photocatalyst than rutile? - Model studies on epitaxial TiO₂ films, *Sci. Rep.*, 2014, **4**, 4043.
- [12] M. Rafique, S. HajraMuneeb, I. Muhammad, U. Muhammad, I.Mohammad, A. A. Waqar, M. Ashraf. Hydrogen Production Using TiO₂-Based Photocatalysts: A Comprehensive Review, *ACS Omega* 2023, **29**, 25640–25648.
- [13] M. Batzill. Fundamental aspects of surface engineering of transition metal oxide photocatalysts. *Energy Environm. Sci.*, 2011,**4**, 3275-86.
- [14] J.N. Wilson, H. Idriss. Structure sensitivity and photocatalytic reactions of semiconductors. Effect of the last layer atomic arrangement. *J. Am. Chem. Soc.*, 2002,**124**, 11284–85.
- [15] M. Xu. Photocatalytic activity of bulk TiO₂ anatase and rutile single crystals using infrared absorption spectroscopy. *Phys. Rev. Lett.*, 2011,**106**, 138302.
- [16] H. Tang, K. Prasad, R. Sanjines, P.E. Schmid, F. Levy, Electrical and optical properties of TiO₂ anatase thin films. *J. Appl. Phys.*, 1994,**75**, 2042.
- [17] L.Thulin, J. Guerra. Calculations of strain-modified anatase TiO₂ band structures. *Phys. Rev. B*, 2008,**77**, 195112.
- [18] J.Joy, J.Mathew, S.C. George. Nanomaterials for photoelectrochemical water splitting-Review. *Int. J. Hydrog. Energy*, 2018,**43**, 4804-17.
- [19] P. Kumar, P. Devi, R. Jain, S.M. Shivaprasad, R.K. Sinha, G. Zhou, R. Nötzel. Quantum dot activated, indium gallium nitride on silicon as photoanode for solar hydrogen generation. *Commun. Chem.* 2019,**2**, 4.
- [20] T. Le, K.Mawatari, Y.Pihosh, T.Kawazoe, T.Yatsui, M. Ohtsu, M. Tosa, T. Kitamori. Optical near-field induced visible response photoelectrochemical water splitting on nanorod TiO₂. *Appl. Phys. Lett.*, 2011, **99**, 213105.



- [21] B. Li, Q. Li, B. Gupta, Z. Guan, L. Zhang, M. Zhang, J. Yang. Space-induced charge carriers separation enhances photocatalytic hydrogen evolution on hollow urchin-like TiO₂ nanomaterial, *J. Alloys compd.*, 2020, **837**, 155547.
- [22] H. Eidsvåg, S. Bentouba, P. Vajeeston, S. Yohi, D. Velauthapillai. TiO₂ as a Photocatalyst for Water Splitting-An Experimental and Theoretical Review. *Molecules*, 2021, **26**, 1687.
- [23] Y. Pihosh, I. Turkevych, K. Mawatari, N. Fukuda, R. Ohta, M. Tosa, K. Shimamura, E. G. Villora, T. Kitamori. Ubiquitous element approach to plasmonic enhanced water splitting: the case of Ti@TiO₂ core-shell nanostructure. *Nanotechnology*, 2014, **25**, 315402.
- [24] D. P. Kumara, V. D. Kumarib, M. Karthik, M. Sathishd, M.V. Shankar. Shape dependence structural, optical and photocatalytic properties of TiO₂ nanocrystals for enhanced hydrogen production via glycerol reforming, *Solar Energy Materials & Solar Cells*, 2017, **163**, 113–119.
- [25] N. Murakami, S. Kawakami, T. Tsubotaa, T. Ohno. Dependence of photocatalytic activity on particle size of a shape-controlled anatase titanium (IV) oxide nanocrystal, *Journal of Molecular Catalysis A: Chemical*, 2012, **358**, 106–111.
- [26] Y.K. Kho, A. Iwase, W.Y. Teoh, L. Mädler, A. Kudo, R. Amal. Photocatalytic H₂ Evolution over TiO₂ Nanoparticles. The Synergistic Effect of Anatase and Rutile, *J. Phys. Chem. C*, 2010, **114**, 2821–29.
- [27] H.H.Do, D.L.T. Nguyen, X.C. Nguyen, T.H. Le, T.P. Nguyen, Q.T. Trinh, S.H. Ahn, D.V.N.Vo, S.Y. Kim, Q.V. Le. Recent progress in TiO₂-based photocatalysts for hydrogen evolution reaction: A review, *Arabian Journal of Chemistry*, 2020, **13**, 3653-71.
- [28] S. Pokrant, S. Dilger, S. Landsmann, M. Trottmann. Size effects of cocatalysts in photoelectrochemical and photocatalytic water splitting. *Mater. Today Energy.*, 2017, **5**, 158-63.
- [29] J. Schneider, M. Matsuoka, M. Takeuchi, J. Zhang, Y. Horiuchi, M. Anpo, D. W. Bahnemann. Understanding TiO₂ Photocatalysis: Mechanisms and Materials, *Chem. Rev.*, 2014, **114**, 9919–9986.
- [30] Y. Wang, L. Li, X. Huang, Q. Li, G. Li. New insights into fluorinated TiO₂ (brookite, anatase and rutile) nanoparticles as efficient photocatalytic redox catalysts. *RSC Adv.*, 2015, **5**, 34302.
- [31] N.D. Johari, Z.M. Rosli, J. M. Juoi, S.A. Yazid. Comparison on the TiO₂ crystalline phases deposited via dip and spin coating using green sol–gel route. *J. Mater. Res. Technol.*, 2019, **8**, 2350-58.
- [32] W. Hu, L. Li, W. Tong, G. Li, Supersaturated Spontaneous Nucleation to TiO₂ Microspheres: Synthesis and Giant Dielectric Performance. *Chem. Comm.*, 2010, **46**, 3113–15.
- [33] S. Sadhu, P. Gupta, P. Poddar. Physical Mechanism Behind Enhanced Photoelectrochemical and Photocatalytic Properties of Superhydrophilic Assemblies of 3D-TiO₂ Microspheres with Arrays of Oriented, Single-Crystalline TiO₂ Nanowires as Building Blocks Deposited on Fluorine-Doped Tin Oxide. *ACS Appl. Mater. Interfaces.*, 2017, **9**, 11202–11.



- [34] K.S. Kim, J.K. Kim, W.S. Kim. Influence of reaction conditions on sol-precipitation process producing silicon oxide particles. *Ceram. Int.*, 2002, **28**, 187-194.
- [35] A.E. Danks, S.R. Hall, Z. Schnepf. The evolution of ‘sol-gel’ chemistry as a technique for materials synthesis. *Mater. Horiz.*, 2016, **3**, 91.
- [36] C.T. Dinh, T.D. Nguyen, F. Kleitz, T.O. Do. Shape-Controlled Synthesis of Highly Crystalline Titania Nanocrystals. *ACS Nano*, 2009, **3**, 3737–3743.
- [37] S.Sadhu, P. Poddar. Template-Free Fabrication of Highly Oriented Single-Crystalline 1D Rutile TiO₂-MWCNT Composite for Enhanced Photoelectrochemical Activity, *J. Phys. Chem. C.*, 2014,**118**, 19363–19373.
- [38] E.M. Huseynov, E.A. Huseynova. Infrared spectroscopy of nanocrystalline anatase (TiO₂) particles under neutron irradiation, *Opt. Mater.*, 2023,**144**, 14351.
- [39] T. Hisatomi, J.Kubota, K. Domen. Recent advances in semiconductors for photocatalytic and photoelectrochemical water splitting, *Chem. Soc. Rev.*, 2014, **43**, 7520.
- [40] R. Shwetharani, M. Sakar, C. A. N. Fernando, V. Binasc R. Geetha Balakrishna. Recent advances and strategies to tailor the energy levels, active sites and electron mobility in titania and its doped/composite analogues for hydrogen evolution in sunlight, *Catal. Sci. Technol.*, 2019, **9**, 12.
- [41] D.O.Scanlon, C.W. Dunnill, J.Buckeridge, S.A. Shevlin, A.J. Logsdail, S. Woodley, M. Richard, C. Catlow, A. Powell, M.J. Palgrave, R.G. Parkin, I.P. Watson, G.W. Keal, T.W. Sherwood, P. Walsh, A. Sokol. Band alignment of rutile and anatase TiO₂, *Nat. Mater.*, 2013, **12**, 798–801.
- [42] K. Zakrzewska. Nonstoichiometry in TiO_{2-y} Studied by Ion Beam Methods and Photoelectron Spectroscopy, *Adv. Mater. Sci. Eng.*, 2012, **826873**, 1-13.
- [43] B. Dong, J Cui, , Y, Qi, F. Zhang, Nanostructure Engineering and Modulation of (Oxy)Nitrides for Application in Visible-Light-Driven Water Splitting. *Adv. Mater.*, 2021, **33**, 2004697.
- [44] B. Gupta, A. Aziz, S. Sundriyal, V. Shrivastav, A.A. Melvin, M. Holdynski, W. Nogala, *Sci. Rep.*,2023,**13**, 5019.
- [45] S.F. Shaikh, R.S. Mane, B.K. Min, Y.J. Hwang, O.S. Joo. D-sorbitol-induced phase control of TiO₂ nanoparticles and its application for dye-sensitized solar cells. *Sci. Rep.*,2015,**6**, 20103.
- [46] O. Fontelles-Carceller, M.J. Muñoz-Batista, E. Rodríguez-Castellón, J.C. Conesa, M. Fernández-García, A. Kubacka. Measuring and interpreting quantum efficiency for hydrogen photo-production using Pt-titania catalysts. *J. Catal.*, 2017, **347**, 157-69.
- [47] S.E.Salas, B.S.Rosales, H.de Lasa, Quantum yield with platinum modified TiO₂ photocatalyst for hydrogen production, *Appl. Catal. B: Environ.*, 2013,**140**, 523-36



[48] B. Wang, D.H.C. Wan, A.T.F. Cheung, D.Y.C. Leung, X.Y. Lu, M.K.H. Leung. Green hydrogen production by solar photocatalysis using Pt-TiO₂ nanosheets with reactive facets *HKIE Transactions*, 2021,**28**, 75-81.

[49] E.P. Melian, C.R.Lopez, A.O. Mendez, O.G. Diaz, M.N. Suarez, J.M.D Rodriguez, J.A. Navio, , D.F. Hevia, Hydrogen production using Pt-loaded TiO₂ photocatalyst. *Int. J. Hydro. Energy*, 2013,**38**, 11737-748.



Data availability

Data will be made available on request

